

# Electronic Structure and Optical Properties of Mixed Iodine/Bromine Lead Perovskites. To Mix or Not to Mix?

Valentin Diez-Cabanes,\* Jacky Even, David Beljonne, and Claudio Quarti

Halide mixing is a key strategy to tune the emission wavelength in lead halide perovskites but is also effective in improving the performance of halide perovskite solar cells. Yet, a clear and global picture of how halide alloying and related spatial in/homogeneous distribution influence the electronic and optical properties of halide perovskites is currently lacking. Considering the preeminent mixed iodine/bromine perovskite as a case study, state-of-the-art hybrid density functional theory calculations are performed, exploring the full space of chemical composition and accounting for phase segregation effects. It is shown that, at low doping regime, halide impurities do not act as trap states and that a quasi-linear opening of the bandgap occurs with increasing the bromine content. Phase segregation at the nanoscale, in turn, drastically affects the electronic structure of mixed halide systems, with namely bromine rich domains acting as barrier to hole diffusion. The energetic disorder probed by optical absorption in these mixed systems is surprisingly insensitive to configurational disorder, but mostly dominated by the coexistence of phases with various degrees of halide segregation.

decade.<sup>[1–4]</sup> Their suitable direct gap, long diffusion length, small exciton binding energy, and easy processability make such materials promising candidates to be integrated in optoelectronic devices such as photovoltaic solar cells (PVs)<sup>[5–8]</sup> or light emitting diodes (LEDs).<sup>[9–11]</sup> Probably the most remarkable feature of MH materials is their apparent resilience to both static and dynamic energetic disorder, as evinced namely by sharp electronic transitions measured both in absorption and emission. Indeed, this finding is very surprising considering the ultrasoft nature of this class of semiconductors<sup>[12]</sup> as well as the fact that MH films are often prepared from solution. Most notably, independent estimates of the Urbach tail<sup>[13]</sup> from photothermal deflection spectroscopy<sup>[14]</sup> and UV–vis absorption spectroscopy<sup>[15–17]</sup> indicate energetic disorder for the band-to-band transition of  $\approx 15$  meV at room

temperature in  $\text{CH}_3\text{NH}_3\text{PbI}_3$  halide perovskite, which is comparable to data reported for highly crystalline inorganic semiconductors such as GaAs or InP.<sup>[17]</sup>

MH perovskites present an  $\text{ABX}_3$  chemical structure, where the A cations are immersed in a lattice of  $\text{BX}_6$  octahedra connected in a corner-sharing fashion. The chemical constituents typically comprise methylammonium ( $\text{MA}^+$ ), formamidinium ( $\text{FA}^+$ ), or  $\text{Cs}^+$  as A cations,  $\text{Pb}^{2+}$  or  $\text{Sn}^{2+}$  atoms as B metal cations, and a halide ( $\text{I}^-$ ,  $\text{Br}^-$ , and  $\text{Cl}^-$ ) as  $\text{X}^-$  anion. Even with a limited number of different cations and anions, the final composition of the material can take multiple forms going beyond the simple, fully inorganic tricomponent systems (like  $\text{CsPbI}_3$ ), including mixed halides (with  $\text{MAPbX}_3$  stoichiometry). Compared to the corresponding single halide materials, mixed halide perovskites show improved morphology and stability together with tunable photophysical response.<sup>[18–20]</sup> For example, the room-temperature electronic bandgaps of the single halide  $\text{MAPbX}_3$  phases amount to 1.6, 2.3, and 2.9 eV for  $\text{X} = \text{I}$ ,  $\text{Br}$ , and  $\text{Cl}$ , respectively.<sup>[21–23]</sup> Very interestingly, a close to linear dependence of the bandgaps with the I versus Br or Cl content has been reported in homogeneously mixed halide perovskites by Noh et al.<sup>[24]</sup> and by Sadhanala et al.,<sup>[14]</sup> hence paving the way to bandgap engineering on demand.<sup>[24–27]</sup> Notice also that layered perovskites exhibit similar behaviors despite the additional importance of strong exciton binding at room temperature.<sup>[28]</sup>

Intuitively, one would expect that mixing various halides would yield either increased electronic disorder (with formation of shallow or deep trap states) or/and structural disorder (with

## 1. Introduction


Hybrid metal halide (MH) perovskites have been under intense scrutiny for their semiconducting properties during the last

Dr. V. Diez-Cabanes, Prof. D. Beljonne, Dr. C. Quarti  
Laboratory for Chemistry of Novel Materials  
University of Mons—UMONS  
Place du Parc 20, Mons 7000, Belgium  
E-mail: valentin.diez-cabanes@univ-lorraine.fr

Dr. V. Diez-Cabanes  
Universite de Lorraine  
CNRS  
Laboratoire de Physique et Chimie Théoriques (LPCT)-UMR 7019  
Nancy F-54000, France

Prof. J. Even  
Univ Rennes  
INSA Rennes  
CNRS  
Institut FOTON-UMR 6082  
Rennes F-35000, France

Dr. C. Quarti  
Univ Rennes  
ENSCR  
INSA Rennes  
CNRS  
ISCR (Institut des Sciences Chimiques de Rennes)-UMR 6226  
Rennes F-35000, France

 The ORCID identification number(s) for the author(s) of this article can be found under <https://doi.org/10.1002/adom.202001832>.

DOI: 10.1002/adom.202001832

segregation of Br- vs I-rich phases). Indeed, halide segregation is an additional source of complexity, resulting change of the optical and electronic properties of mixed halide perovskite during time. Many studies highlighted the dependence of this phenomenon with many variables, including material composition, light irradiation,<sup>[29]</sup> applied voltage,<sup>[30]</sup> or thermal activation.<sup>[31]</sup> As a matter of fact, the segregation of halide phases in these materials has been evidenced by light emission spectroscopy, with the apparition of two peaks corresponding to the I-rich and Br-rich regions. The origin of halide segregation in MAPbI<sub>3-x</sub>Br<sub>x</sub> samples is still under debate with many different mechanisms proposed in the literature.<sup>[32]</sup> From a thermodynamic standpoint, the formation of Br-rich regions has been reported to be favorable for a wide range of mixed compositions (15–75% of Br content).<sup>[33]</sup> It has also been pointed out that a defect mediated migration via iodine vacancies could initiate the formation of iodine segregated phases at the grain boundaries.<sup>[34]</sup> There are also literature data supporting the view that the lattice strain prompted by exciton (polaron) formation can be released by the creation of I- and Br- segregated regions.<sup>[35]</sup> Although these mechanistic studies are useful to identify strategies for preventing halide segregation during device operation,<sup>[36]</sup> here we *assume* phase segregation occurs over various length scales and predict how it affects the electronic structure of the mixed halide materials, irrespective of its origin. This induced ion migration leads to the formation of unwanted halide defects<sup>[37]</sup> that can be prevented by means of oxygen passivation,<sup>[38]</sup> iodine treatment,<sup>[39]</sup> or the use of long-chain ammonium ligand capped crystallites.<sup>[40]</sup> The decrease in device performances induced by halide segregation has been related to trapping in the I-rich spatial domains.<sup>[41]</sup> On the contrary, intimately mixed halide perovskites exhibited sharp optical edges (as measured from spectral tails) with Urbach energies similar to those in the pure phases, at least at small content in Br (in the order of 20%).<sup>[14]</sup> Understanding how the presence of more halide species and their distribution in real samples (finely interdispersed or segregated) influences the electronic and optical properties of metal halide perovskites is definitely crucial. Earlier theoretical works have been dedicated to the comparison of the electronic structure of pure iodine and bromine systems,<sup>[42–44]</sup> while subsequent works focused on specific halide compositions, such as FA<sub>0.8</sub>MA<sub>0.2</sub>PbI<sub>2.4</sub>Br<sub>0.6</sub> in ref. [45] and MAPbI<sub>2.97</sub>Cl<sub>0.03</sub> in ref. [46], or made use of simplified schemes to study the electronic properties of mixed halide systems. In ref. [47], in particular, Jong et al. studied the electronic structure of mixed iodine/bromine lead solid state solutions, making use of the virtual crystal approximation. This method enables to tackle solid-state solutions for any concentration of chemical impurities, including the smallest one, but at the cost of neglecting disorder-induced correlation effects and therefore losing important atomistic details. Thus, questions about the potential formation of trap states related to halide impurities, the global evolution of the optical and transport properties of mixed halide perovskites across chemical space, or the influence of phase segregation over various scales have remained unanswered. Inspired by these questions, we present here a comprehensive density functional theory (DFT) study of how the electronic structure of mixed lead halide perovskites evolves with chemical composition and segregation, considering iodine/bromine mixtures as case study,

in light of their relevance for light-emission<sup>[48,49]</sup> and photovoltaic<sup>[50,51]</sup> applications and for the abundance of literature studies.<sup>[14,20,24,37,45,47]</sup> We first discuss the influence of halide impurities with respect to the electronic structure of pure phase halide perovskites (Section 2.1). Then, we present the evolution of the electronic and transport properties of mixed halide solid state solutions for all chemical compositions ranging from pure iodine to pure bromine phases, also addressing the effect of phase segregation (Sections 2.2 and 2.3, respectively). Finally, we analyze the effect of the halide composition and (in)homogeneity on the optical properties (Section 2.4) and sum up the main findings (Section 3).

## 2. Results and Discussion

### 2.1. Pure and Dilute Lead Halide Perovskites Alloys

We start by analyzing the effect of halide impurities in otherwise pure phase compounds. To this aim, we performed periodic DFT simulations considering first pure halide MAPbI<sub>3</sub> and MAPbBr<sub>3</sub> phases, then substituting one halide atom in the cell. For the simulation of pure phase materials, we adopted the tetragonal I4/mcm structure, accessible from 162 K to room temperature and between 155 and 237 K for MAPbI<sub>3</sub> and MAPbBr<sub>3</sub>,<sup>[52]</sup> respectively (see the Supporting Information), therefore representing a useful common reference for these two compounds. Atomic positions were fully relaxed at Perdew–Burke–Ernzerhof (PBE) level of theory, with cell parameters kept fixed at the corresponding experimental values reported from X-ray diffraction (XRD) measurements.<sup>[52]</sup> This level of theory is well known to fortuitously reproduce the bandgap of MAPbI<sub>3</sub> because of error cancellation.<sup>[53]</sup> In fact, the correct bandgap is retrieved once accurately accounting properly for electronic correlation effects (i.e., via hybrid DFT or many-body approaches based on the GW approximation (being *G* the time-ordered one-body Green's function, and *W* the screened Coulomb potential)) and when including spin orbit coupling (SOC) corrections. To achieve a quantitative description of the electronic properties of mixed halide perovskites, we resort here to SOC-corrected hybrid density functional theory.<sup>[53,54]</sup> Unless stated otherwise, the hybrid PBE0 exchange-correlation functional was adopted, as it has been shown to provide accurate bandgaps both for 3D<sup>[55]</sup> and layered 2D perovskites.<sup>[56]</sup> We further analyzed how the bandgaps for the pure phase materials evolves with the amount of Hartree–Fock exchange (see Figure S12, Supporting Information), finding that 25% exact-exchange provides bandgap values in excellent agreement with experiment for MAPbI<sub>3</sub> (1.7 eV calculated vs 1.6 eV measured from UV–vis spectroscopy<sup>[57]</sup>) and slightly underestimated for MAPbBr<sub>3</sub> (2.12 eV calculated vs and 2.3 eV measured<sup>[57]</sup>). Noteworthy, many-body calculations based on the GW approximations, as performed by Mosconi et al., provided similar bandgap for MAPbI<sub>3</sub> (1.7 eV), but significantly overestimated the bandgap of MAPbBr<sub>3</sub> (2.59 eV).<sup>[44]</sup> It is also worth stressing that the room temperature exciton binding energy in 3D halide perovskite is generally very small, measured in the range from 9 to 15 meV,<sup>[58]</sup> hence making the valence-to-conduction gap obtained from DFT a good approximation to the optical bandgap obtained experimentally.

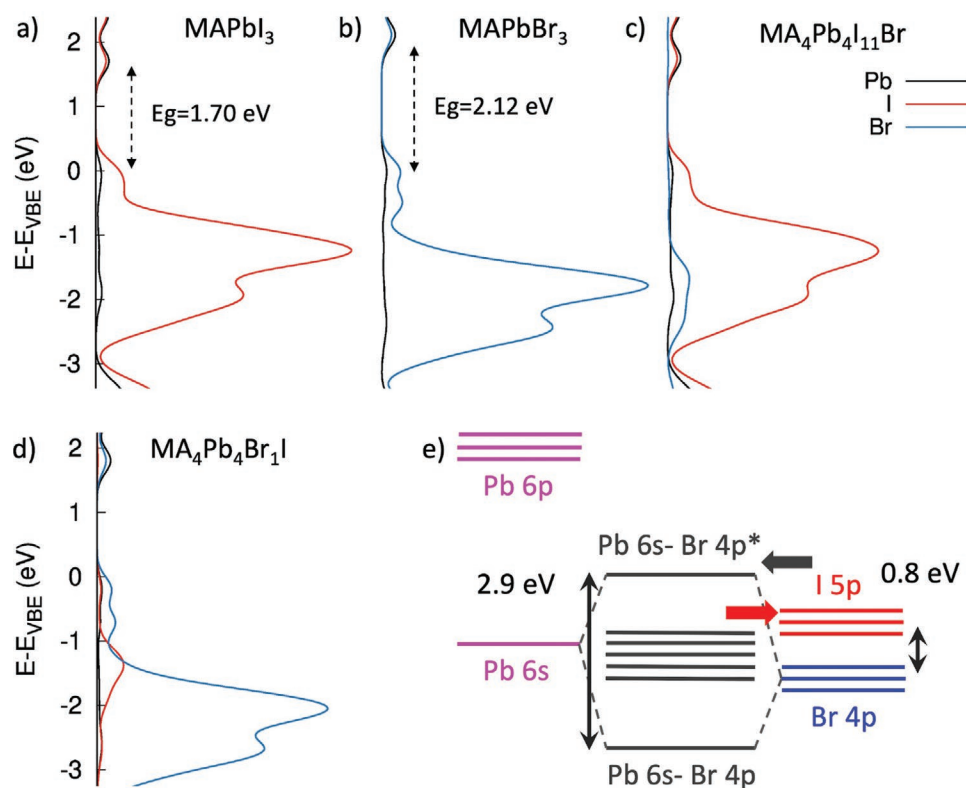


**Figure 1.** a) Atomic projected density of states (pDOS) for pure halide MAPbI<sub>3</sub> and b) MAPbBr<sub>3</sub> compounds, in their corresponding tetragonal phase. c) pDOS for mixed halide MA<sub>4</sub>Pb<sub>4</sub>I<sub>11</sub>Br and d) MA<sub>4</sub>Pb<sub>4</sub>Br<sub>11</sub>I compounds. Contributions from lead, iodine, and bromine atoms are reported in black, red, and blue, respectively. e) Schematics of the hybridization of the atomic orbitals for the valence band, as composed by combination of s-states of lead (magenta) and p-states of the iodine (red) and bromine (blue), along with indication of the valence bandwidth and difference in atomic site energies for Br 4p and I 5p states.

Atomic projected density of states for pure MAPbI<sub>3</sub> and MAPbBr<sub>3</sub> are reported in **Figure 1a,b**, respectively. In line with previous reports from the literature, our calculations on pure halide perovskites show that the conduction band edge is composed by antibonding combination of Pb 6p and Xs orbitals with predominant Pb contributions, while the valence band (VB) is composed by antibonding combination of Pb 6s and Xp orbitals.<sup>[59,60]</sup> Corresponding band structures as computed at PBE level of theory including SOC are reported in Figure S13 in the Supporting Information. As a result, substitution of one halide in the tetragonal cell is expected to affect mainly the VB edge. The substitution of one halogen atom in the tetragonal cell of the pure phase structures takes two different colors, MA<sub>4</sub>Pb<sub>4</sub>I<sub>11</sub>Br and MA<sub>4</sub>Pb<sub>4</sub>Br<sub>11</sub>I. In the case of MA<sub>4</sub>Pb<sub>4</sub>I<sub>11</sub>Br, the 4p orbitals of the Br dopant are lower in energy with respect to the 5p orbitals of the bulk I atoms, hence the replacement of one I by one Br is expected to result in the formation of Br-related levels lying deep inside the VB of the parental MAPbI<sub>3</sub> lattice. This argument is confirmed by our calculations (see Figure 1c), which highlights the presence of bromine related levels ≈ 2 eV below the valence band edge. A more interesting case is MA<sub>4</sub>Pb<sub>4</sub>Br<sub>11</sub>I, where the higher-lying 5p orbitals of the I dopant could potentially pull out electronic levels above the valence band edge, with resulting formation of trap states, generally associated to diminished performances in optoelectronic devices. However, our solid-state calculations show that in MA<sub>4</sub>Pb<sub>4</sub>Br<sub>11</sub>I (Figure 1d),

as in MA<sub>4</sub>Pb<sub>4</sub>I<sub>11</sub>Br, the iodine-related orbitals remain completely immersed in the valence band, hence no trapping of the hole carriers should occur at reasonable charge density. This is also evident from the band structures in the Figure S13 in the Supporting Information, which all show well dispersed bands both for the pure and mixed halide compounds. A discrete resonance associated to a single impurity with a different on-site energy, may appear outside the continuous density of states related to the 3D unperturbed lattice electronic band dispersion in simplified tight-binding modeling.<sup>[61]</sup> Unfortunately, the 3D tight-binding model for the 3D perovskite lattice,<sup>[60]</sup> although yielding an analytical expression for the energy of the valence band maximum (VBM) at the R, does not allow a full computation of unperturbed perovskite lattice Green function. It is known nevertheless that a discrete resonance generally appears if the ratio between the difference of on-site energies and the bandwidth, exceeds a given threshold (this threshold is equal to 1/2 for s orbitals in a simple cubic monoatomic lattice).<sup>[61]</sup> The “clean gap” in MA<sub>4</sub>Pb<sub>4</sub>Br<sub>11</sub>I results from the strong lead-halide hybridization and the large width of the Pb 6s-Br 4p band (≈ 2.9 eV) that largely overcomes the on-site energy differences between the I 5p and the Br 4p levels (of ≈ 0.8 eV), as depicted in Figure 1e. We note that the strong antibonding character at the valence band edge has also been largely evoked in the literature to explain the resilience of lead halide perovskites against trapping at localized states associated with point defects.<sup>[62,63]</sup>

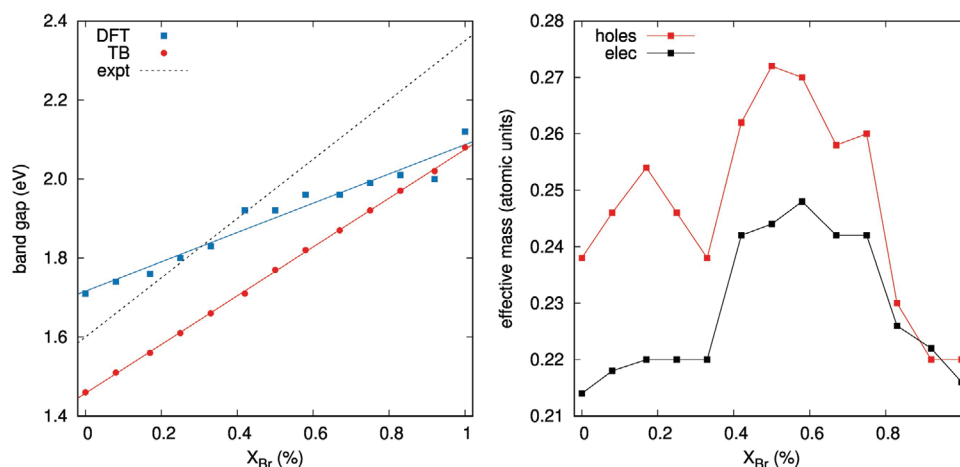


**Figure 2.** a) Evolution of the bandgap for mixed iodine/bromine lead perovskites, with respect to bromine content, as estimated from hybrid DFT simulations (DFT), from simplified tight-binding Hamiltonian (TB, vide infra) and measured experimentally (expt). b) Evolution of the average effective masses of holes (black) and electrons (red), with respect to bromine content. Effective masses have been averaged along five different directions, related to the crystalline axes  $\Gamma \rightarrow (001)$ ,  $\Gamma \rightarrow (010)$ ,  $\Gamma \rightarrow (001)$  of the tetragonal cell and along the pseudocubic  $\Gamma \rightarrow (1 \pm 10)$  axes.

## 2.2. Halide Solid-State Solutions

We now move to mixed halide systems with iodine: bromine chemical composition tuned continuously from 100:0% to 0:100%, considering the most generic case of finely mixed iodine/bromine solid state solution. To this aim, we considered the tetragonal cell of  $\text{MAPbI}_3$  as reference model and progressively substituted iodines with bromines, avoiding configurations showing spatially segregated Br and I phases. For pure halide phases, cell parameters have been kept fixed to experimental values,<sup>[39]</sup> while for mixed halide compositions, these have been linearly interpolated with respect to the bromine content, in line with XRD measurements<sup>[24,25]</sup> (additional test by relaxing the cell have been performed, resulting in very similar trends, see Figure S14, Supporting Information). For all these structures, we performed full relaxations of the atomic positions using PBE exchange-correlation functional and then provided accurate estimates of the band single-particle gaps, adopting the same hybrid PBE0 approach (including SOC) as proposed in Section 2.1. The evolution of the computed bandgaps as function of the bromine content is reported in Figure 2a, showing a general opening of the bandgap with increase in bromine content, in agreement with earlier experimental results reported first by Noh et al.<sup>[24]</sup> The trend in Figure 2a can be explained by assuming an “ensemble” picture where contributions from iodine and bromine ions are averaged according to the overall chemical composition. This can be easily modeled using a simplified tight-binding Hamiltonian, where the on-site energies of the halide s-/p- orbitals are gradually tuned between those of the outer shell iodine 5s/5p and bromine 4s/4p orbitals (more details on the computational parameters can be found in the Supporting Information). Adopting the symmetry-based simple tight-binding model and parameterization developed earlier,<sup>[60]</sup> we indeed recover a close to linear dependence of the computed bandgap with bromine/iodine ratio, see Figure 2a. In fact, it is possible to demonstrate analytically that, in absence of SOC, the trend should be quadratic but with a very small curvature (see the Supporting Information). Noteworthy, a similar

picture for mixed halide perovskites solid state solutions was recently proposed by Jong et al. using DFT simulations based on the virtual crystal approximation.<sup>[47]</sup> Overall, our theoretical results thus support the view that, in samples featuring homogeneous distributions of Br and I atoms (solid-state solutions), the energy gap can be engineered at will via halide composition.

An additional question deals with the effect of halide mixing on transport properties. To assess this, we have computed the band structures and effective masses for the same mixed halide models, here resorting to the PBE level of theory (including SOC effects). Comparable hybrid calculations for the band dispersion would be highly coveted, but these are unfortunately out of reach, at least for the 48 atoms tetragonal model investigated here. Components of the effective mass tensors for both holes and electrons have been computed along the directions of the three crystalline axes and along the pseudocubic  $\langle 1 \pm 10 \rangle$  axes and are listed in Table S12 in the Supporting Information. Global electron and hole effective masses, as averaged along the five abovementioned crystalline directions, are depicted in Figure 2b. The calculated values in the pure systems  $\text{MAPbI}_3$  and  $\text{MAPbBr}_3$  are in the range 0.19–0.24  $m_e$ , in good agreement with similar DFT calculations from literature.<sup>[54,64,65]</sup> Interestingly, the averaged hole and electron effective masses are only modestly affected (within less than 20%) by large variations in chemical space, showing a tiny maximum around 50/50 halide compositions, indicating that chemical disorder in halide composition should have a mild impact on transport properties in this class of mixed halide perovskites. The effect is slightly more evident for holes than for electrons, in line with the fact that valence band is mainly composed by p-orbitals of the halides. We may also notice that layered perovskites exhibit only small modifications of the exciton resonance in mixed compounds at room temperature, which might indicate that in-plane effective masses are not strongly affected by alloying.<sup>[28]</sup> The resulting moderate reduction of the exciton resonance was rather attributed to an increase of the photoluminescence (PL) linewidth in alloys similar to the present findings for 3D compounds (vide infra).

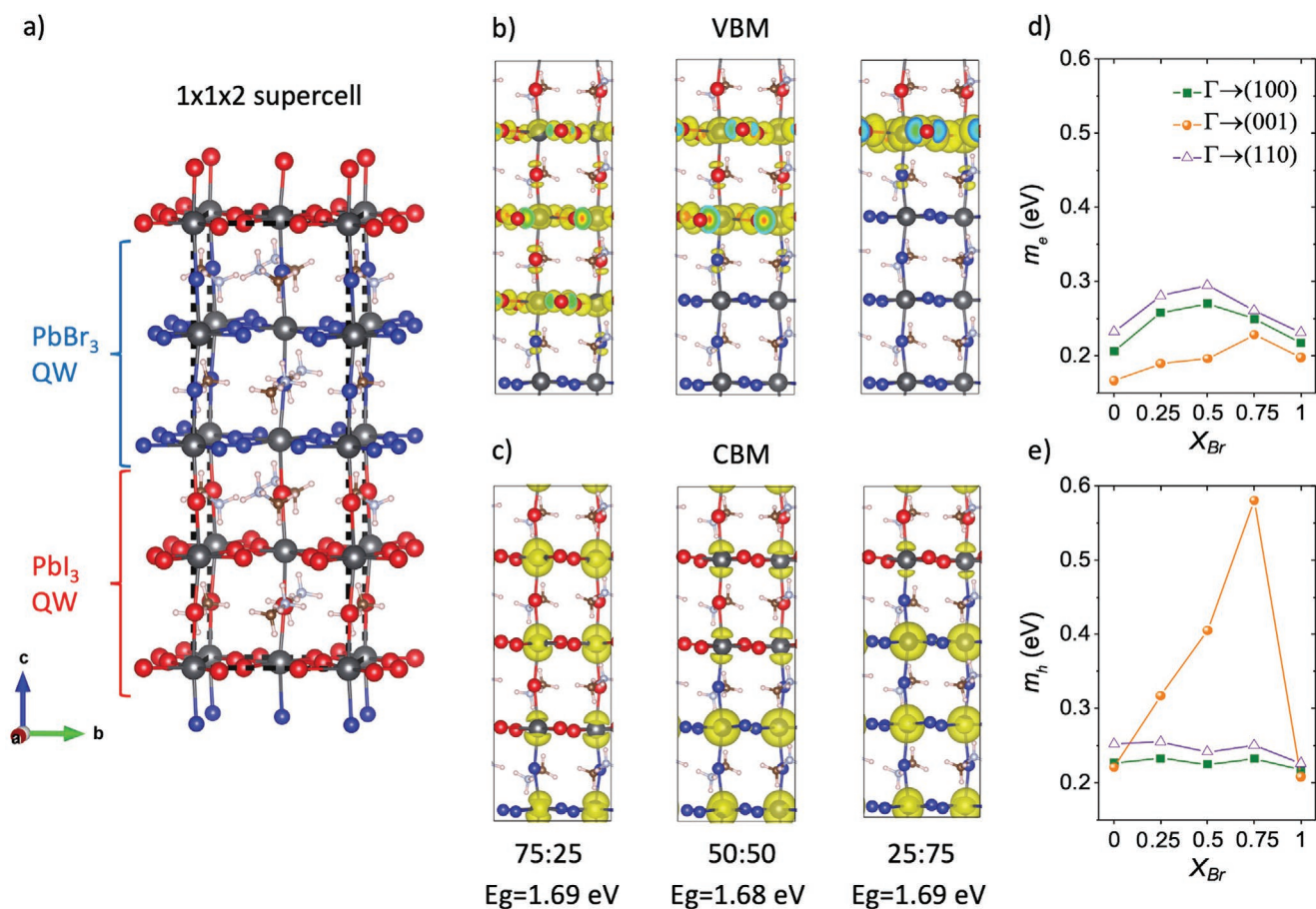


**Figure 3.** a)  $1 \times 1 \times 2$  supercell model adopted to investigate halide segregation in mixed halide states. b) Spatial delocalization of the valence band maximum, VBM and c) conduction band maximum, CBM as function of the iodine: bromine composition. d) Evolution of the effective mass electron and e) of the hole along in-plane  $\langle 100 \rangle$  and  $\langle 110 \rangle$  directions and out-of-plane  $\langle 001 \rangle$  direction, as function of the iodine:bromine composition.

At last, one may expect that inhomogeneous strain distribution, as related to compressive strain close to the iodide atoms and tensile strain close to the bromide atoms, can play a role in dictating the electronic/transport properties of the alloy.<sup>[66]</sup> Indeed, structural analysis of our fully relaxed periodic models reveals sporadic but sizable distortions in the lead-halide bond length, compared to those of pure phases (see Figure S15, Supporting Information). This effect shall lead to deviations from the quasi-linear behavior of the bandgap as a function of the composition and explains the oscillations of the bandgap for our fully relaxed DFT models in Figure 2.

### 2.3. Halide Segregated Systems

We here turn our attention to the effect of halide segregation on the electronic properties of mixed halide perovskites. For this purpose, we have adopted a reference  $1 \times 1 \times 2$  supercell of the tetragonal phase of  $\text{MAPbX}_3$ , containing four layers with  $\text{PbX}_3$  composition stacked along the  $c$ -axis. Within this cell, halide segregation can be easily introduced as shown in Figure 3a, by constructing two layers with  $\text{PbI}_3$  and  $\text{PbBr}_3$  compositions and variable thickness, resembling quantum-well (QW) structures stacked along the tetragonal  $c$ -axis. We therefore constructed

quantum-well like models with reciprocal thickness of three  $\text{PbI}_3$  and one  $\text{PbBr}_3$  layer (iodine: bromine composition 75%:25%), two  $\text{PbI}_3$  and two  $\text{PbBr}_3$  layers (50%:50%), one  $\text{PbI}_3$  and three  $\text{PbBr}_3$  layers (25%:75%). In spite of its simplicity, this 1D model for halide segregation is able to grasp important effects associated to halide segregation at the scale of a few nm, while preserving computational accuracy (hybrid DFT calculations with SOC). We note that morphological studies performed for segregated samples indicate halide rich regions up to 30 nm in size.<sup>[35]</sup> Realistic modeling of such large spatial domains from first-principles remains, unfortunately, computationally prohibitive and the focus here is on trends that already manifest at the nm scale.

In striking contrast to the mixed halide case, characterized by bandgap opening with increasing bromine composition (Figure 2a), all the segregated halide models investigated here show a bandgap of  $\approx 1.68$ – $1.69$  eV, quite close to that of the pure iodine phase, irrespectively from the bromine content in the cell. This behavior can be rationalized by examining the nature of the frontier crystalline orbitals, shown in Figure 3b,c. While the VBM is clearly localized in the  $\text{PbI}_3$  layer (Figure 3b), the conduction band minimum (CBM) tends to spread on both the iodine and bromine layers (Figure 3c). Bromine-related occupied levels appear deeper in the valence band and likely

contribute to higher-energy optical transitions (see Figure S16, Supporting Information). The present theoretical results agree with experimental reports. Indeed, Sadhanala et al. reported PL emission in mixed halide perovskite sample with nominal composition  $\text{CH}_3\text{NH}_3\text{PbI}_{1.8}\text{Br}_{1.2}$  (40% bromine) quite close to that of pure iodine phase, 1.65 eV versus 1.57 eV, respectively.<sup>[14]</sup> Similar findings were later reported by Barker et al. who observed PL redshifts in two samples of  $\text{CH}_3\text{NH}_3\text{PbX}_3$  with nominal 40% and 60% bromine content, from 1.8 and 1.95 eV, respectively, down to 1.7 eV, again close to the emission in the pure iodine phase.<sup>[37]</sup> These authors associated the evolution of the PL under light-soaking to induced halide migration, supported by earlier reports of ionic mobility in halide perovskite from impedance spectroscopic measurements<sup>[67]</sup> and other techniques.<sup>[29,68–70]</sup> Very interestingly, our theoretical results in Figure 3 suggest that changes in the optical properties of mixed halide perovskites are already effective for phase segregation on the scale of few nanometers. Among various other effects, that due to quantum confinement of the two  $\text{MAPbI}_3$  by the  $\text{MAPbBr}_3$  is worth singling out. Such an effect likely explains the small increase of the bandgap in the  $\text{MAPbI}_3$  by comparison to the related bulk value. Notably, local strains invoked above should result in compressive deformation in the  $\text{MAPbI}_3$  region, mitigating the bandgap increase. However, structural analysis indicates that lead-iodine bond lengths do not significantly deviate in the segregated models, as compared to pure phases (see Figure S17, Supporting Information).

With the localization of the electronic states reflecting the local halide composition, one can anticipate phase segregation to significantly influence the transport properties of mixed halide perovskites. To quantify this, we computed electron and hole effective masses for all the investigated iodine: bromine compositions, considering the  $\langle 100 \rangle$  and  $\langle 110 \rangle$  directions within the quantum-well plane (corresponding to the  $a$ -axis, and the pseudo-cubic axis, respectively) and along the quantum-well stacking  $\langle 001 \rangle$  direction (corresponding to the  $c$ -axis). Also in this case, because of the impossibility to resort to hybrid DFT calculations for estimating the band dispersion in these models, we adopted PBE exchange-correlation functional along with SOC. Electron effective masses in Figure 3d show overall weak dependence with respect to halide composition, on similar ground to what found for solid state halide solution in Figure 2b. This effect is evident both within the  $\langle 100 \rangle$  and  $\langle 110 \rangle$  directions within the quantum-well and along the stacking  $\langle 001 \rangle$  direction and is consistent with the spatial delocalization of the crystalline states at the conduction band minimum across the iodine/bromine boundary. Hole effective masses, instead, show significant changes in the  $\langle 001 \rangle$  quantum-well stacking direction (but no effects in the  $\langle 100 \rangle$  and  $\langle 110 \rangle$  planes) (Figure 3e). Not unexpectedly, compared to pure  $\text{MAPbI}_3$ , the increase in the hole effective mass is only modest (by about 40%) in the case of 75:25% iodine: bromine composition, corresponding to a single  $\text{PbBr}_3$  layer separating the  $\text{PbI}_3$  layers, which indicates that tunneling effects mediated either by tailing of the wavefunctions or superexchange interactions are still operational. This quickly deteriorates when increasing the thickness of the tunneling region, with up to a threefold increase in the hole effective mass for 25:75% iodine: bromine composition (corresponding to a

one-layer thick  $\text{PbI}_3$  quantum well separated from its periodic replica by three layers of  $\text{PbBr}_3$ ). The emerging picture is that a layer-by-layer segregation of the halides should significantly impede transport of the holes in the vertical stacking direction for phase segregation occurring over length scales as small as a few layers (nm), while electron diffusion should remain largely unaffected. Corresponding experimental demonstration of the detrimental effect of halide segregation on perovskite transport properties has not been reported yet, at least to the best of our knowledge. However, improved transport properties have been recently reported in mixed halide perovskites wherein phase segregation is hindered by introducing small contents of chlorine.<sup>[71]</sup> Photoconductivity transient transport measurements performed on the resulting, homogeneously mixed, triple halide perovskites indeed showed larger charge carrier mobility and extended lifetimes in comparison with the reference  $\text{APbI}_{2.4}\text{Br}_{0.6}$  material.

#### 2.4. Optoelectronic Properties with Heterogeneous Halide Distribution

In this section, we model the optical properties of mixed halide perovskites as a function of chemical heterogeneity. To do so, we used a  $2 \times 2 \times 2$  supercell model of the tetragonal phase of  $\text{MAPbX}_3$  (384 atoms, 32 chemical units) and fix the overall composition to a one-to-one (50%:50%) iodine: bromine ratio. As the present model is too large to allow for hybrid DFT calculations including SOC, the calculations are performed at the PBE level.<sup>[53,54]</sup> To smoothly interpolate from halide segregated to solid state solution phases, we have built successive models by randomly exchanging  $n$  iodine-bromine pairs starting from the pure QW segregated structure. As there are 96 halide atoms (48 Br and 48 I) in the supercell, we have constructed systems of increasing degree of phase segregation by performing from  $n = 0$  (QW segregated system) up to  $n = 24$  (solid-state solution) atom exchanges, as schematized in Figure 4a. Moreover, for each value of  $n$ , 20 randomly generated structures were considered in order to build statistically representative results. First, we note that our DFT calculations yield very similar (within the accuracy of the model) total energies per unit cell in the segregated versus mixed structures, so we expect these to coexist in the real films (see Figure S18, Supporting Information).

Figure 4b shows the evolution of the bandgap with the degree of mixing  $n$ , as averaged over the 20 models considered. This shows a monotonic increase ( $\approx 0.1$  eV) from the segregated phase ( $n = 0$ ) to the solid-state solution ( $n = 24$ ), hence smoothly bridging the results obtained between these two extreme cases in Sections 2.2 and 2.3, respectively. This finding goes in line with the light-triggered redshift of 0.2 eV observed by Barker et al. in the PL spectra in  $\text{MAPbI}_{3-x}\text{Br}_x$  ( $x = 0.5$ ) samples, as obtained from the extrapolation for the values reported for  $x = 0.4$  and  $x = 0.6$  compositions.<sup>[37]</sup> The standard deviation at different degree of mixing  $n$  is, to a large extent, independent of  $n$ . Namely the exchange of four iodine-bromine pairs in the quantum-well model as randomly realized over 20 structures results in an energetic disorder of 28 meV (standard deviation), compared to 31 meV for 24 exchanges. Because they are of similar stability, the cumulative standard deviation accounting

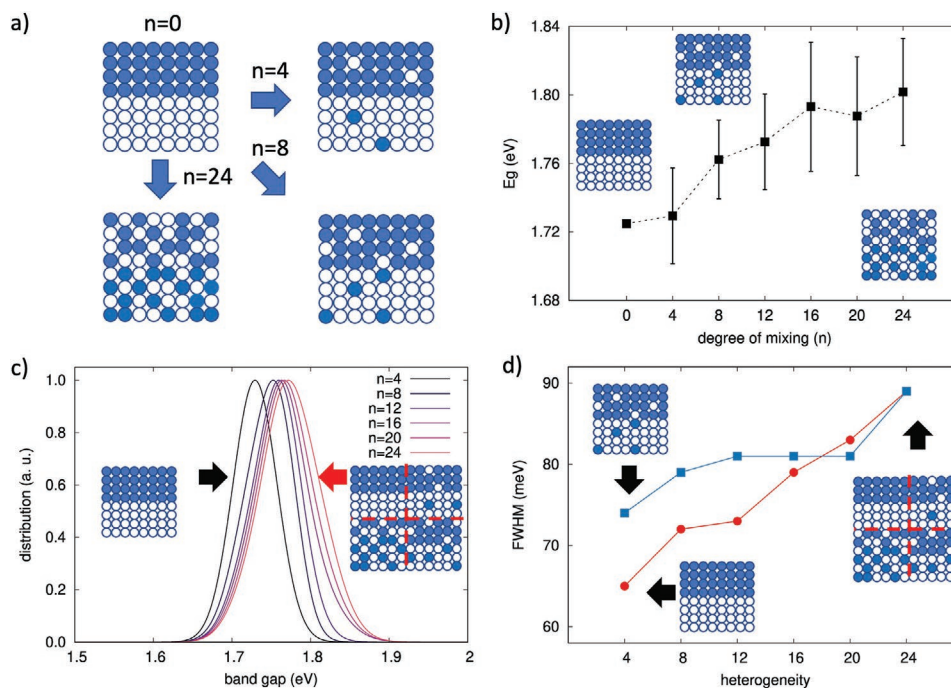


**Figure 4.** a) Schematics for the mixing parameter  $n$ , for the sampling of mixed halide systems with intermediate halide distributions between the quantum-well case ( $n = 0$ ) and the solid state solution case ( $n = 24$ ). Fixed 50:50 halide concentration. b) Average bandgaps for systems with different degree of mixing  $n$ , as computed from 20 realizations of  $n$  halide exchanges. The error-bar on the energy axis corresponds to the standard deviation. c) Gaussian distributions obtained by cumulating over the degrees of mixing ( $n = 4$  and  $n = 8$  and so on). d) Full width half maximum (FWHM) associated to the cumulative distributions. Red and blue data refer to cumulative distributions starting from  $n = 4$  (quantum-well like structure) or from  $n = 24$  (solid state solution like).

(see Figure S19, Supporting Information), on an equal footing, for various degrees of phase segregation might be a more representative metric for the amount of disorder. The resulting cumulated distributions in bandgaps are shown in Figure 4c. Two remarkable results emerge from the data. Compared to the completely phase-segregated  $n = 0$  (bilayer) model, i) the peak of the distribution progressively blueshifts and ii) the width of the distribution increases with increasing spatial heterogeneity in halide composition. The corresponding full-width-half-maximum (FWHM), reported in Figure 4d, indeed increases by 50% (from 65 to 89 meV) when going from the quasi-pure  $n = 4$  model to the cumulative distribution including all degrees of mixing (from  $n = 4$  to  $n = 24$ ). The same analysis can, of course, be performed now considering the solid-state solution ( $n = 24$ ) as a reference model, and accounting for an increasing number of segregated configurations (from  $n = 20$  down to  $n = 4$ ) in the ensemble, and results in a similar increase in the FWHM from 70 to 89 meV. Although based on very simple statistical arguments, the theoretical predictions are fully consistent with experimental data from Sadhanala et al., who reported an increase in the FWHM of the PL signal from  $\approx 100$  meV in pure  $\text{CH}_3\text{NH}_3\text{PbI}_3$  phase to  $\approx 140$  meV in nominal  $\text{CH}_3\text{NH}_3\text{PbI}_{1.8}\text{Br}_{1.2}$  (bromine 40%).<sup>[14]</sup> In layered perovskite alloys, the exciton PL linewidth for intermediate compositions was interpreted on the basis of similar statistical arguments.<sup>[28]</sup> Most importantly, our analysis suggests that the main culprit for the increased broadening in the PL signal of mixed halide phases, compared to the corresponding pure phases, is not merely associated with the larger number of accessible chemical configurations afforded

by the *amount* of mixing (as this quickly saturates at relatively low degree of halide mixing, Figure 4b), but is rather dictated by the coexistence of mixed phases with various *spatial degrees of halide segregation*. While our work highlights broadening of the optical absorption spectrum as the signature for phase inhomogeneity in mixed halide perovskites, this is not the unique fingerprint.<sup>[36]</sup> Namely, small fractions of segregated phase (on the order of 1%)<sup>[72]</sup> have been shown to severely hinge on light emission<sup>[29]</sup> and photovoltaic response.<sup>[30,41,72]</sup> Further experimental characterization is needed to correlate these changes in chemical composition with the optoelectronic properties of mixed halide perovskite samples. In that context, we would like to highlight the work by Stavarakas et al., who recently set up a photoluminescence tomographic technique able to probe electron-hole recombination from thick mixed halide perovskite samples with  $\mu\text{m}$  lateral resolution,<sup>[73]</sup> and independent studies by Vela et al.<sup>[74]</sup> and Roiland et al.<sup>[75]</sup> demonstrating the ability of solid-state NMR to characterize the halide composition of mixed halide perovskites, as well as the formation of segregated phases, at the scale of individual  $\text{PbX}_6$  octahedra.

### 3. Conclusions

Halide mixing has been demonstrated to be a very effective strategy to tune the optical properties of halide perovskites materials while improving their performance and stability<sup>[18–20]</sup> Future developments of mixed halide perovskite materials and related devices hinge on the basic understanding of how halide

composition influences the electronic structure and optical properties of these materials. We have reported a comprehensive computational study based on periodic density functional theory calculations of mixed iodine: bromine lead perovskites, paying particular attention to the importance of short-range phase segregation going all the way from finely intermixed to spatially separated phases. We have first shown that sparse halide substitution does not introduce trap states in the band structure, appearing as another manifestation for the often invoked defect tolerance of lead halide materials.<sup>[62,63]</sup> The electronic structure of solid-state halide solutions shows a continuous evolution with iodine: bromine composition ranging from 100:0% to 0:100%, with namely a quasi-linear opening of the bandgap with increasing bromine content. This confirms that the bandgap of intimately mixed halide perovskite can be tuned at will with chemical composition as, in this case, the materials of mixed composition behave essentially as weighted average of the two pure phases. On the other hand, halide segregation strongly influences the optical and transport properties of mixed halide perovskite semiconductors. Namely, the effective bandgap of the fully segregated iodine: bromine mixtures reduces to that of the smaller bandgap material, namely MAPbI<sub>3</sub>, and a large increase in hole effective mass occurs for spatial segregation over only a few nanometer length scales. The emerging picture is that halide segregation can severely impact balanced transport and collection of electrons and holes at the electrodes and suggest the need for a fine control of the morphology in mixed iodine-bromine systems to guarantee a continuous percolation pathway for thermalized holes. Investigations on the effect of halide mixing on the optical properties show that the dominating contribution to the increased broadening in mixed halides stems from the coexistence of phases with various degrees of spatial halide segregation rather than from configurational disorder. While additional effects should be considered to achieve a thorough understanding of the spectral lineshapes in mixed halide perovskites (namely the role of thermal distortions of the lattice), this work represents a first step toward a comprehensive picture for the energy landscape explored by charge carriers in these materials and the possible identification of strategies toward reduced recombination losses in actual device configurations. In this context, referring to the question raised in the title, our calculations suggest that what matters the most is not so much the amount of mixing (relative ratio of iodine and bromine ions in mixed domains, see Section 2.4) but rather the length scale over which the phase segregation occurs (see Section 2.3). Phase segregation over microscopic (a few nm) distances is, according to our calculations, detrimental to transport and prone to nonradiative recombination (as reflected by the increased effective masses and larger energetic disorder, respectively). Yet, a complete separation between I- and Br-rich phases stabilized through the use of mixed organic cations has been shown to cause charge accumulation and the formation of p- and n-photodoped regions, turning into efficient light emission (with photoluminescence quantum efficiencies up to 41%) at low charge injection.<sup>[76]</sup> Note, however, that the phase segregation in the MAPbI<sub>3-x</sub>Br<sub>x</sub> materials investigated here, mimicking few nm halide-rich clusters embedded into an homogeneously mixed halide matrix,<sup>[35]</sup> differs from the photodoping work by Feldmann et al.,<sup>[76]</sup> where the two halide phases are completely separated in μm-size domains.

## 4. Experimental Section

All DFT calculations were performed using a pseudopotential/plane wave formalism, as implemented in the Quantum-Espresso suite program.<sup>[77]</sup> Structural relaxations were performed for all the investigated systems using the PBE functional<sup>[78]</sup> for the description of the exchange-correlation energy, along with ultrasoft pseudopotentials (PPs) and wavefunction/density cutoffs of 25/200 Rydberg. Electronic properties were computed instead adopting norm-conserving along with 50/200 Ry cutoffs and including spin-orbit coupling (SOC). Band structure and electron/hole effective masses were estimated with PBE functional along with a 4 × 4 × 4 sampling of the First Brillouin zone following the Monkhorst-Pack scheme.<sup>[79]</sup> To achieve quantitative estimates of the electronic bandgap of pure iodine and bromine perovskites and intermediate Br/I compositions, additional calculations were performed using the hybrid PBE0 functional<sup>[80]</sup> and including SOC. Such a method (including 25% of exact exchange) indeed yields bandgaps of 1.70 and 2.12 eV for MAPbI<sub>3</sub> and MAPbBr<sub>3</sub>, in good agreement with experimental data (1.6 and 2.3 eV, respectively, see Figure S12 in the Supporting Information for the test of the exchange-correlation (xc) fraction). Because of their large computational cost, hybrid functional calculations were performed only at the  $\Gamma$ -point of the Brillouin zone.

For the pure phases, cell parameters were set to the values obtained from XRD measurements.<sup>[52]</sup> For mixed systems, cell parameters were obtained from linear extrapolation of the pure MAPbI<sub>3</sub> and MAPbBr<sub>3</sub> systems (see Figure S14, Supporting Information).

## Supporting Information

Supporting Information is available from the Wiley Online Library or from the author.

## Acknowledgements

This work was financially supported by the project RW-FEDER-SOLIDYE-2 (grant agreement (GA) No. 1510616). Computational resources were provided by the Consortium des Équipements de Calcul Intensif (CÉCI) funded by the Belgian National Fund for Scientific Research (F.R.S.-FNRS) under Grant 2.5020.11 and by Tier-1 supercomputer of the Fédération Wallonie-Bruxelles, infrastructure funded by the Walloon Region under the Grant Agreement No. 1117545. D.B. is an FNRS research director. J.E. is a senior member of Institut Universitaire de France. C.Q. acknowledges the Agence Nationale de la Recherche (ANR) funded MORELESS project (ANR-18-CE05-0026) for financial support.

## Conflict of Interest

The authors declare no conflict of interest.

## Keywords

halide mixing, hybrid organometal halide perovskites, optical broadening, transport properties

Received: October 22, 2020

Revised: December 11, 2020

Published online:

[1] H. J. Snaith, *J. Phys. Chem. Lett.* **2013**, *4*, 3623.

[2] T. M. Brenner, D. A. Egger, L. Kronik, G. Hodes, D. Cahen, *Nat. Rev. Mater.* **2016**, *1*, 15007.



- [3] J. S. Manser, J. A. Christians, P. V. Kamat, *Chem. Rev.* **2016**, *116*, 12956.
- [4] B. Saparov, D. B. Mitzi, *Chem. Rev.* **2016**, *116*, 4558.
- [5] M. Grätzel, *Nat. Mater.* **2014**, *13*, 838.
- [6] J. P. Correa-Baena, M. Saliba, T. Buonassisi, M. Grätzel, A. Abate, W. Tress, A. Hagfeldt, *Science* **2017**, *358*, 739.
- [7] A. K. Jena, A. Kulkarni, T. Miyasaka, *Chem. Rev.* **2019**, *119*, 3036.
- [8] P. K. Nayak, S. Mahesh, H. J. Snaith, D. Cahen, *Nat. Rev. Mater.* **2019**, *4*, 269.
- [9] B. R. Sutherland, E. H. Sargent, *Nat. Photonics* **2016**, *10*, 295.
- [10] S. D. Stranks, H. J. Snaith, *Nat. Nanotechnol.* **2015**, *10*, 391.
- [11] Z. K. Tan, R. S. Moghaddam, M. L. Lai, P. Docampo, R. Higler, F. Deschler, M. Price, A. Sadhanala, L. M. Pazos, D. Credgington, F. Hanusch, T. Bein, H. J. Snaith, R. H. Friend, *Nat. Nanotechnol.* **2014**, *9*, 687.
- [12] A. C. Ferreira, A. Létoublon, S. Paofai, S. Raymond, C. Ecolivet, B. Rufflé, S. Cordier, C. Katan, M. I. Saidaminov, A. A. Zhumekenov, O. M. Bakr, J. Even, P. Bourges, *Phys. Rev. Lett.* **2018**, *121*, 085502.
- [13] F. Urbach, *Phys. Rev.* **1953**, *92*, 1324.
- [14] A. Sadhanala, F. Deschler, T. H. Thomas, S. E. Dutton, K. C. Goedel, F. C. Hanusch, M. L. Lai, U. Steiner, T. Bein, P. Docampo, D. Cahen, R. H. Friend, *J. Phys. Chem. Lett.* **2014**, *5*, 2501.
- [15] S. De Wolf, J. Holovsky, S. J. Moon, P. Löper, B. Niesen, M. Ledinsky, F. J. Haug, J. H. Yum, C. Ballif, *J. Phys. Chem. Lett.* **2014**, *5*, 1035.
- [16] C. Barugkin, J. Cong, T. Duong, S. Rahman, H. T. Nguyen, D. Macdonald, T. P. White, K. R. Catchpole, *J. Phys. Chem. Lett.* **2015**, *6*, 767.
- [17] M. Ledinsky, T. Schönfeldová, J. Holovský, E. Aydin, Z. Hájková, L. Landová, N. Neyková, A. Fejfar, S. De Wolf, *J. Phys. Chem. Lett.* **2019**, *10*, 1368.
- [18] G. E. Eperon, S. D. Stranks, C. Menelaou, M. B. Johnston, L. M. Herz, H. J. Snaith, *Energy Environ. Sci.* **2014**, *7*, 982.
- [19] D. Shi, V. Adinolfi, R. Comin, M. Yuan, E. Alarousu, A. Buin, Y. Chen, S. Hoogland, A. Rothenberger, K. Katsiev, Y. Losovyj, X. Zhang, P. A. Dowben, O. F. Mohammed, E. H. Sargent, O. M. Bakr, *Science* **2015**, *347*, 519.
- [20] N. J. Jeon, J. H. Noh, W. S. Yang, Y. C. Kim, S. Ryu, J. Seo, S. Il Seok, *Nature* **2015**, *517*, 476.
- [21] N. Kitazawa, Y. Watanabe, Y. Nakamura, *J. Mater. Sci.* **2002**, *37*, 3585.
- [22] Y. Yamada, T. Nakamura, M. Endo, A. Wakamiya, Y. Kanemitsu, *Appl. Phys. Express* **2014**, *7*, 5.
- [23] G. Maculan, A. D. Sheikh, A. L. Abdelhady, M. I. Saidaminov, M. A. Haque, B. Murali, E. Alarousu, O. F. Mohammed, T. Wu, O. M. Bakr, *J. Phys. Chem. Lett.* **2015**, *6*, 3781.
- [24] J. H. Noh, S. H. Im, J. H. Heo, T. N. Mandal, S. Il Seok, *Nano Lett.* **2013**, *13*, 1764.
- [25] B. W. Park, B. Philippe, S. M. Jain, X. Zhang, T. Edvinsson, H. Rensmo, B. Zietz, G. Boschloo, *J. Mater. Chem. A* **2015**, *3*, 21760.
- [26] L. Gil-Escrig, A. Miquel-Sempere, M. Sessolo, H. J. Bolink, *J. Phys. Chem. Lett.* **2015**, *6*, 3743.
- [27] L. Atourki, E. Vega, B. Marí, M. Mollar, H. Ait Ahsaine, K. Bouabid, A. Ihlal, *Appl. Surf. Sci.* **2016**, *371*, 112.
- [28] G. Lanty, K. Jemli, Y. Wei, J. Leymarie, J. Even, J. S. Lauret, E. Deleporte, *J. Phys. Chem. Lett.* **2014**, *5*, 3958.
- [29] E. T. Hoke, D. J. Slotcavage, E. R. Dohner, A. R. Bowering, H. I. Karunadasa, M. D. McGehee, *Chem. Sci.* **2015**, *6*, 613.
- [30] I. L. Braly, R. J. Stoddard, A. Rajagopal, A. R. Uhl, J. K. Katahara, A. K. Y. Jen, H. W. Hillhouse, *ACS Energy Lett.* **2017**, *2*, 1841.
- [31] T. Elmeland, R. A. Scheidt, B. Seger, P. V. Kamat, *ACS Energy Lett.* **2019**, *4*, 1961.
- [32] M. C. Brennan, S. Draguta, P. V. Kamat, M. Kuno, *ACS Energy Lett.* **2018**, *3*, 204.
- [33] F. Brivio, C. Caetano, A. Walsh, *J. Phys. Chem. Lett.* **2016**, *7*, 1083.
- [34] S. J. Yoon, M. Kuno, P. V. Kamat, *ACS Energy Lett.* **2017**, *2*, 1507.
- [35] C. G. Bischak, C. L. Hetherington, H. Wu, S. Aloni, D. F. Ogletree, D. T. Limmer, N. S. Ginsberg, *Nano Lett.* **2017**, *17*, 1028.
- [36] A. J. Knight, L. M. Herz, *Energy Environ. Sci.* **2020**, *13*, 2024.
- [37] A. J. Barker, A. Sadhanala, F. Deschler, M. Gandini, S. P. Senanayak, P. M. Pearce, E. Mosconi, A. J. Pearson, Y. Wu, A. R. Srimath Kandada, T. Leijtens, F. De Angelis, S. E. Dutton, A. Petrozza, R. H. Friend, *ACS Energy Lett.* **2017**, *2*, 1416.
- [38] W. Fan, Y. Shi, T. Shi, S. Chu, W. Chen, K. O. Ighodalo, J. Zhao, X. Li, Z. Xiao, *ACS Energy Lett.* **2019**, *4*, 2052.
- [39] R. G. Balakrishna, S. M. Kobosko, P. V. Kamat, *ACS Energy Lett.* **2018**, *3*, 2267.
- [40] Z. Xiao, L. Zhao, N. L. Tran, Y. L. Lin, S. H. Silver, R. A. Kerner, N. Yao, A. Kahn, G. D. Scholes, B. P. Rand, *Nano Lett.* **2017**, *17*, 6863.
- [41] G. F. Samu, C. Janáky, P. V. Kamat, *ACS Energy Lett.* **2017**, *2*, 1860.
- [42] J. Even, L. Pedesseau, C. Katan, M. Kepenekian, J. S. Lauret, D. Saporì, E. Deleporte, *J. Phys. Chem. C* **2015**, *119*, 10161.
- [43] K. T. Butler, J. M. Frost, A. Walsh, *Mater. Horiz.* **2015**, *2*, 228.
- [44] E. Mosconi, P. Umari, F. De Angelis, *Phys. Chem. Chem. Phys.* **2016**, *18*, 27158.
- [45] J. C. Brauer, D. Tsokkou, S. Sanchez, N. Droseros, B. Roose, E. Mosconi, X. Hua, M. Stollerfoht, D. Neher, U. Steiner, F. De Angelis, A. Abate, N. Banerji, *J. Chem. Phys.* **2020**, *152*, 104703.
- [46] C. Quarti, E. Mosconi, P. Umari, F. De Angelis, *Inorg. Chem.* **2017**, *56*, 74.
- [47] U. G. Jong, C. J. Yu, J. S. Ri, N. H. Kim, G. C. Ri, *Phys. Rev. B* **2016**, *94*, 125139.
- [48] M. Abdi-Jalebi, Z. Andaji-Garmaroudi, S. Cacovich, C. Stavrakas, B. Philippe, J. M. Richter, M. Alsari, E. P. Booker, E. M. Hutter, A. J. Pearson, S. Lilliu, T. J. Savenije, H. Rensmo, G. Divitini, C. Ducati, R. H. Friend, S. D. Stranks, *Nature* **2018**, *555*, 497.
- [49] N. K. Kumawat, X. K. Liu, D. Kabra, F. Gao, *Nanoscale* **2019**, *11*, 2109.
- [50] Y. Zhou, F. Wang, H. H. Fang, M. A. Loi, F. Y. Xie, N. Zhao, C. P. Wong, *J. Mater. Chem. A* **2016**, *4*, 16191.
- [51] H. F. Zarick, N. Soetan, W. R. Erwin, R. Bardhan, *J. Mater. Chem. A* **2018**, *6*, 5507.
- [52] A. Poglitsch, D. Weber, *J. Chem. Phys.* **1987**, *87*, 6373.
- [53] J. Even, L. Pedesseau, J. M. Jancu, C. Katan, *J. Phys. Chem. Lett.* **2013**, *4*, 2999.
- [54] P. Umari, E. Mosconi, F. De Angelis, *Sci. Rep.* **2014**, *4*, 4467.
- [55] J. Wiktór, U. Rothlisberger, A. Pasquarello, *J. Phys. Chem. Lett.* **2017**, *8*, 5507.
- [56] C. Quarti, N. Marchal, D. Beljonne, *J. Phys. Chem. Lett.* **2018**, *9*, 3416.
- [57] P. Schulz, E. Edri, S. Kirmayer, G. Hodes, D. Cahen, A. Kahn, *Energy Environ. Sci.* **2014**, *7*, 1377.
- [58] A. Miyata, A. Mitioglu, P. Plochocka, O. Portugall, J. T. W. Wang, S. D. Stranks, H. J. Snaith, R. J. Nicholas, *Nat. Phys.* **2015**, *11*, 582.
- [59] T. Umabayashi, K. Asai, T. Kondo, A. Nakao, *Phys. Rev. B: Condens. Matter Mater. Phys.* **2003**, *67*, 2.
- [60] S. Boyer-Richard, C. Katan, B. Traoré, R. Scholz, J. M. Jancu, J. Even, *J. Phys. Chem. Lett.* **2016**, *7*, 3833.
- [61] E. N. Economou, *Green's Functions in Quantum Physics*, 3rd ed., Springer Series in Solid-State Sciences, Vol. 7, Springer, Berlin, Heidelberg **2006**.
- [62] K. X. Steirer, P. Schulz, G. Teeter, V. Stevanovic, M. Yang, K. Zhu, J. J. Berry, *ACS Energy Lett.* **2016**, *1*, 360.
- [63] J. Kang, L. W. Wang, *J. Phys. Chem. Lett.* **2017**, *8*, 489.
- [64] F. Brivio, K. T. Butler, A. Walsh, M. Van Schilfgaarde, *Phys. Rev. B: Condens. Matter Mater. Phys.* **2014**, *89*, 155204.
- [65] S. T. A. G. Melissen, F. Labat, P. Sautet, T. Le Bahers, *Phys. Chem. Chem. Phys.* **2015**, *17*, 2199.
- [66] H. Tsai, R. Asadour, J.-C. Blancon, C. C. Stoumpos, O. Durand, J. W. Strzalka, B. Chen, R. Verduzco, P. M. Ajayan, S. Tretiak, J. Even,

- M. A. Alam, M. G. Kanatzidis, W. Nie, A. D. Mohite, *Science* **2018**, 360, 67.
- [67] E. J. Juarez-Perez, R. S. Sanchez, L. Badia, G. Garcia-Belmonte, Y. S. Kang, I. Mora-Sero, J. Bisquert, *J. Phys. Chem. Lett.* **2014**, 5, 2390.
- [68] C. Eames, J. M. Frost, P. R. F. Barnes, B. C. O'Regan, A. Walsh, M. S. Islam, *Nat. Commun.* **2015**, 6, 2.
- [69] P. Delugas, C. Caddeo, A. Filippetti, A. Mattoni, *J. Phys. Chem. Lett.* **2016**, 7, 2356.
- [70] A. Senocrate, I. Moudrakovski, G. Y. Kim, T. Y. Yang, G. Gregori, M. Grätzel, J. Maier, *Angew. Chem., Int. Ed.* **2017**, 56, 7755.
- [71] J. Xu, C. C. Boyd, Z. J. Yu, A. F. Palmstrom, D. J. Witter, B. W. Larson, R. M. France, J. Werner, S. P. Harvey, E. J. Wolf, W. Weigand, S. Manzoor, M. F. A. M. Van Hest, J. J. Berry, J. M. Luther, Z. C. Holman, M. D. McGehee, *Science* **2020**, 367, 1097.
- [72] S. Mahesh, J. M. Ball, R. D. J. Oliver, D. P. McMeekin, P. K. Nayak, M. B. Johnston, H. J. Snaith, *Energy Environ. Sci.* **2020**, 13, 258.
- [73] C. Stavrakas, A. A. Zhumekenov, R. Brenes, M. Abdi-Jalebi, V. Bulović, O. M. Bakr, E. S. Barnard, S. D. Stranks, *Energy Environ. Sci.* **2018**, 11, 2846.
- [74] B. A. Rosales, L. Men, S. D. Cady, M. P. Hanrahan, A. J. Rossini, J. Vela, *Chem. Mater.* **2016**, 28, 6848.
- [75] C. Roiland, G. Trippé-Allard, K. Jemli, B. Alonso, J. C. Ameline, R. Gautier, T. Bataille, L. L. Pollès, E. Deleporte, J. Even, C. Katan, *Phys. Chem. Chem. Phys.* **2016**, 18, 27133.
- [76] S. Feldmann, S. Macpherson, S. P. Senanayak, M. Abdi-Jalebi, J. P. H. Rivett, G. Nan, G. D. Tainter, T. A. S. Doherty, K. Frohna, E. Ringe, R. H. Friend, H. Sirringhaus, M. Saliba, D. Beljonne, S. D. Stranks, F. Deschler, *Nat. Photonics* **2020**, 14, 123.
- [77] P. Giannozzi, S. Baroni, N. Bonini, M. Calandra, R. Car, C. Cavazzoni, D. Ceresoli, G. L. Chiarotti, M. Cococcioni, I. Dabo, A. Dal Corso, S. De Gironcoli, S. Fabris, G. Fratesi, R. Gebauer, U. Gerstmann, C. Gougoussis, A. Kokalj, M. Lazzeri, L. Martin-Samos, N. Marzari, F. Mauri, R. Mazzarello, S. Paolini, A. Pasquarello, L. Paulatto, C. Sbraccia, S. Scandolo, G. Sclauzero, A. P. Seitsonen, A. Smogunov, P. Umari, R. M. Wentzcovitch, *J. Phys.: Condens. Matter* **2009**, 21, 395502.
- [78] J. P. Perdew, K. Burke, M. Ernzerhof, *Phys. Rev. Lett.* **1996**, 77, 3865.
- [79] J. D. Pack, H. J. Monkhorst, *Phys. Rev. B* **1977**, 16, 1748.
- [80] C. Adamo, V. Barone, *J. Chem. Phys.* **1999**, 110, 6158.